Energy Conversion and Management: X 13 (2022) 100162

Contents lists available at ScienceDirect

Energy Conversion and Management: X

journal homepage: www.sciencedirect.com/journal/energy-conversion-and-management-x

Pentyl valerate biofuel from γ-valerolactone in one-pot process: Insights on the key role of acid sites of the catalytic support

Karla G. Martínez Figueredo, Darío J. Segobia, Nicolás M. Bertero *

Catalysis Science and Engineering Research Group (GICIC), Instituto de Investigaciones en Catálisis y Petroquímica (INCAPE), UNL-CONICET, Centro Científico Tecnológico, Paraje El Pozo, Santa Fe (3000), Santa Fe, Argentina

ARTICLE INFO

Keywords:
One-pot
γ-Valerolactone
Pentyl valerate
Biofuel
Acid requirements
Brønsted/Lewis

ABSTRACT

In this work the acid-catalysed reactions involved in the one-pot production of pentyl valerate (PV) from γ-valerolactone (GVL) and pentanol in liquid phase at 523 K, 10 bar of N_2 over acidic catalysts was studied. Two consecutive acid-catalysed reactions must be performed: (1) nucleophilic addition of pentanol (PL) to GVL to form 4-hydroxy pentyl valerate (HPV) and (2) HPV dehydration into pentyl 2-pentenoate (PP), avoiding the undesirable formation of 4-pentoxy pentyl valerate (PPV). It was found that the support activity and selectivity strongly depended on: (i) the nature; (ii) strength; (iii) density of acid sites and (iv) the textural properties of the acid support. Solids containing predominantly Lewis acid sites, such as ZnO/SiO_2, γ-Al_2O_3 and NaY zeolite promote mainly a strong GVL adsorption leading to a relatively high missing carbon balance. Catalysts having mainly surface Brønsted acid sites of medium–high strength, such as HPA/SiO_2, showed a very high activity and selectivity to PP but deactivated dramatically. Zeolites containing at least 40% of Brønsted acidity and strong acid sites promoted remarkably the undesirable intramolecular dehydration of pentanol into pentenes. SiO_2-Al_2O_3, exhibiting a B/(L + B) ratio of 0.21 and a wide strength of acid sites, was more selective to PP than to PPV though the missing carbon balance was high. By calorimetric adsorption and temperature-programmed oxidation adsorption enthalpies of 61.9 and 59.1 Kcal/mol for GVL and PL were obtained, respectively. Besides, by temperature-programmed desorption experiments it was determined that GVL adsorption is irreversible on SiO_2-Al_2O_3, whereas in the case of PL is partially reversible. The effect of the calcination temperature on the product distribution and evolution of the missing carbon balance was also studied over SiO_2-Al_2O_3. These results contribute to the future design of more efficient bifunctional catalytic systems for biofuel production.

1. Introduction

The growing world population and the development of emerging economies have resulted in a dramatic increase in global energy consumption during the 20th century [1]. Although considerable efforts have been made since the beginning of the 21st century for developing alternative and sustainable energy sources, during 2019 and 2020 the participation of fossil fuels in the total energy consumption in United States was about 80% [2]. However, it is important to highlight that during 2011 this participation level in the energy demand was of 87%, indicating that the use of alternative energies is growing at a relatively slow rate. In industrial economies such as United States, an important portion of the total energy demand is consumed by the transportation sector. For example, for 2019 and 2020 transportation purposes accounted for the 28.4 and 26.1% (due to the COVID-19 pandemic) of the total energy consumed in that country, and the 94% of that energy was provided by fossil fuels. Biomass-derived biofuels contributed only about 5% [2]. Nevertheless, the well-known increasing concern about climate change, associated to greenhouse emissions, is motivating researchers to develop promising biofuels for replacing fossil fuels as soon as possible. The most attractive renewable fuels, from the point of view of their non-food uses and low carbon footprint, are the second-generation biofuels, obtained from the abundant, relatively cheap and renewable lignocellulosic biomass [3]. The main strategy to transform biomass-derived raw materials into biofuels in biorefineries is based on: a) deconstruction of lignocellulose and conversion into platform molecules such as levulinic acid (LA) and γ-valerolactone (GVL); b) transformation of these platform chemicals into biofuels and/or valuable products [4]. In particular GVL has attracted considerable attention in the last years, converting this lactone into a strategic platform molecule

* Corresponding author.
E-mail address: nbertero@fiq.unl.edu.ar (N.M. Bertero).

https://doi.org/10.1016/j.ecmx.2021.100162
Received 26 September 2021; Received in revised form 8 December 2021; Accepted 9 December 2021
Available online 16 December 2021

for obtaining biofuels [4–6]. In particular, Yan et al. [4] published a review on potential applications regarding the upgrading of GVL to fuel additives, diesel fuels and value-added chemicals, where the necessity of improving the biofuel productivity in one-pot processes was highlighted.

A particular type of biofuels called "valeric biofuels" based on valerate esters have shown interesting fuel properties such as: (a) considerable energy densities, (b) more appropriate polarities than current biofuels such as ethanol and (c) appropriate volatility-ignition properties that make these esters compatible for gasoline or diesel pools, depending on their alkyl group. For instance, pentyl valerate (PV) exhibits a better volatility, cold-flow properties and lubricity benefits than fatty acid methyl esters (FAME) [7], and it can be blended with diesel up to 20% without a significant impact on emissions and engine efficiency [8].

Lange et al. reported a novel production of PV and its use as biofuel>10 years ago using bifunctional catalysts based on noble metals, comprising the following reactions: (i) conversion of GVL into pentanoic acid (PA); (ii) esterification of PA with pentanol (PL) [7]. A few years later, Chan-Thaw et al. proposed another one-pot process from GVL and an excess of PL, based on bifunctional copper catalysts [c]. Both types of processes, shown in Fig. 1 (Route 1 and Route 2, respectively), have attracted considerable attention exploring different alternatives for the presence of acid and metal sites in the bifunctional catalyst. The first approach involves the use of an acid support where metal particles are deposited by different methods, mainly impregnation. The second approach, using a non-acidic support such as SiO_2, or a weakly acidic solid as SiO_2-ZrO_2, requires a preparation process leading to metal particles that provide both metal and Lewis acid sites. This second method, exclusively tested in the case of Cu-based catalysts, requires a fine tuning of the morphology of the particles to increase the required acid site density. [9,10]. On the other hand, the first approach allows a wider range of options for selecting the acid and metal function, though some interaction between metal and acid sites can take place modifying the acid/metal balance. Although this type of bifunctional catalysts seems to be the most studied, the role of the acid sites has not been carefully investigated for the acid-catalysed reactions involved in the one-pot process, especially when an excess of PL is used. In this process, the first acid-catalysed reaction involving the ring-opening of GVL, takes place by nucleophilic addition of PL to the carboxylic group of GVL to produce a key and a very reactive intermediate called 4-hydroxy pentyl valerate (HPV). Consecutively, HPV must be dehydrated, also over acid sites, into pentyl 2-pentenoate (PP). Finally, this ester containing a C=C double bond should be hydrogenated to the desired PV over metallic sites [9,10]. However, depending on the characteristics of the acid catalyst and reaction conditions, the HPV intermediate can also react with another PL molecule to form 4-pentoxy pentyl valerate (PPV), an undesirable product. Another possible undesirable reaction over bifunctional catalysts is the conversion of GVL into 2-methyltetrahydrofurane (MTHF) by hydrogenation and hydrogenolysis. When the first approach is employed, i.e. acid sites provided by an acidic support, the main side product formed over acid sites is PPV. However, at the light that there are three different reactions taking place over acid sites (nucleophilic addition of PL to GVL, dehydration of HPV into PP and etherification of HPV with PL leading to PPV), the comprehension of the role of these sites in each acid-catalysed reaction becomes relevant for a suitable support selection.

We have previously reported the use of SiO_2-Al_2O_3-supported Ni [11] and Ru, Ir and Pt-based [12] catalysts with good results in terms of activity and selectivity, showing that SiO_2-Al_2O_3 is a relatively efficient acid support for this reaction path. Nevertheless, a deeper insight on the role of acid sites in each acid-catalysed reaction, in the absence of metal phase, is desirable and will contribute positively to the understanding and development of novel catalytic processes for valeric biofuel production.

The aim of this work is to investigate the particular role of acid sites in both acid catalysed reactions of Fig. 1 Route 2 and their impact on the fraction of GVL reactant strongly adsorbed on the support. To our knowledge, the specific influence of the nature, density and strength of acid sites present in bifunctional catalysts on the product distribution has not been studied yet for this one-pot process. To achieve this, several acid solids were selected for the study, from non-acidic ones such as SiO_2 to clearly acid solids with different acid site density, strength and nature such as γ-Al_2O_3, ZnO/SiO_2, HPA/SiO_2, and NaY, HY, HMOR zeolites. Furthermore, specific aspects of the interaction between GVL and PL with SiO_2-Al_2O_3 surface were explored by temperature-programmed desorption, oxidation and calorimetric studies that provided valuable information about the role of acid sites in the GVL adsorption and

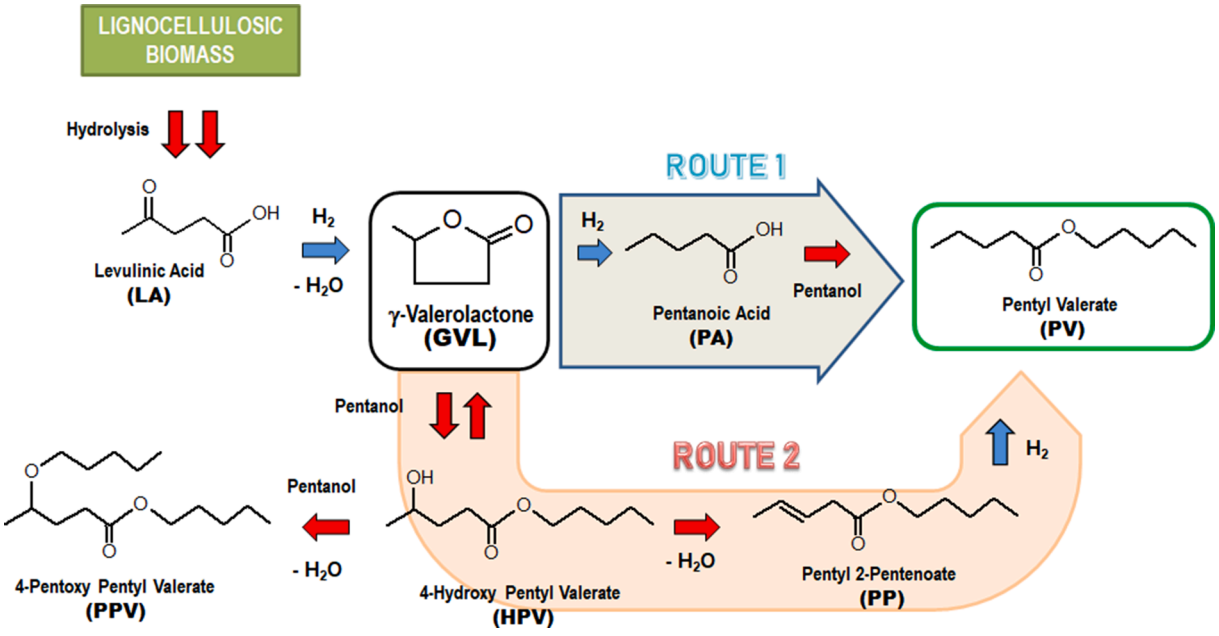

Fig. 1. Reaction network for the one-pot production of pentyl valerate (PV) from biomass-derived γ-valerolactone (GVL), pentanol (PL) and H_2 over bifunctional metal/acid catalysts [→ metal catalyst; →acid catalyst].

conversion into valeric biofuel precursors.

2. Materials and methods

2.1. Materials and catalysts preparation

In the case of SiO_2 (Sigma-Aldrich grade 62, 99.7%), γ-Al_2O_3 (Ketjen CK-300) and SiO_2-Al_2O_3 (Grade 135, 99% Aldrich), the commercial samples were calcined in air flow (60 cm^3/min) at 773 K for 2 h before the characterization and catalytic tests.

ZnO(20%)/SiO_2 sample was prepared by incipient wetness impregnation using the commercial SiO_2 as support and an aqueous solution of $ZnCl_2$ (99.5%, Aldrich), slowly added on the SiO_2 while stirring, as described elsewhere [13]. The catalyst precursor was dried at 373 K for 12 h and then calcined for 2 h in air flow at 623 K.

HPA(42%)/SiO_2 sample was also prepared by incipient wetness impregnation of the commercial SiO_2 with an ethanol/water (50%v/v) solution of $H_3PW_{12}O_{40}{\cdot}6H_2O$ (99.0%, Merck) in order to preserve the Keggin structure [14]. The catalyst precursor was dried at 373 K for 12 h and then calcined for 2 h in a stream of air at 523 K.

Commercial zeolites NaY zeolite (UOP-Y54), and HMOR (Zeocat HZM-760) were calcined in dried air flow at 773 K before the characterization and catalytic tests. HY zeolite was obtained by double ion exchange of the commercial NaY zeolite with a 1 M aqueous solution of NH_4Cl at 353 K, as reported previously [13].

2.2. Catalyst characterization

Elemental composition of the samples was determined by atomic absorption spectroscopy (AAS) in a Perkin Elmer PinAAcle 900T spectrometer and by X-ray fluorescence spectrometry (XRF) in a Shimadzu EDX-720 spectrometer. For determining the textural properties, such as BET surface area (S_g) and mean pore diameter (d_P), N_2 physisorption studies at 77 K were performed in a Quantochrome Corporation NOVA-1000 sorptometer.

Regarding acidic properties, surface acid density (n_A) and relative strength of acid sites were quantified by temperature-programmed desorption (TPD) of NH_3 pre-adsorbed at 373 K on calcined samples as described elsewhere [15]. The total acid site density (n_A) was estimated by deconvolution and integration of the NH_3 desorption profiles. In addition, the nature of surface acid sites was determined by Fourier transform infrared spectroscopy (FT-IR) with a Shimadzu FT-IR-8101M spectrophotometer and using pyridine as probe molecule [15]. The relative contributions of Lewis and Brønsted acid sites were estimated by deconvolution and numerical integration of these pyridine IR absorption bands followed by correction with the corresponding extinction coefficients

The crystalline structure of particular calcined samples (where crystalline species were expected) was verified by X-ray diffraction (XRD) using a Shimadzu XD-1 diffractometer and Ni-filtered Cu-Kα radiation (scan speed 2°/min).

The amount of carbon (coke) deposited on catalysts during calorimetric adsorption experiments was measured by temperature-programmed oxidation (TPO). Catalytic samples were collected from the calorimeter by filtration and then dried at 353 K overnight. Then 15–20 mg of dried sample was treated in N_2 flow for 1 h at 363 K to eliminate weakly adsorbed molecules of GVL, PL or products. Then, samples were heated in a O_2 (2%)/N_2 stream at 10 K min^{-1} from room temperature to 1073 K. The evolved CO_2 was converted into methane in a fixed bed methanation reactor containing a Ni-based catalyst (Ni/kieselguhr) at 673 K and monitored in an SRI 8610C gas chromatograph equipped with a flame ionization detector.

Temperature-programmed desorption of GVL or PL were performed by contacting 100–150 mg of the previously calcined SiO_2-Al_2O_3 with 30 mL of GVL or PL and drying the sample at 373 K for 12 h. Then 100–150 mg of dried sample was treated in N_2 flow for 1 h at 363 K to eliminate weakly adsorbed molecules of GVL or PL. Then, samples were heated in a He stream at 10 K min^{-1} from room temperature to 1073 K. The evolved species were followed by mass spectrometry (MS) in a Baltzers Omnistar unit.

Enthalpies of GVL and PL adsorption on SA were experimentally determined by mixing 1 g of solid sample with 20 mL of GVL or PL in a mechanically stirred calorimeter equipped with a digital thermometer ERTCO-EUTECHNICS 4400 (with a 0.01 K resolution) and using was n-dodecane (Sigma, 99%) as calorimetric fluid. The catalyst samples were previously calcined as described previously. The calorimeter constant was determined by mixing bidistilled water and absolute ethanol (Merck, 99%). The ethanol concentration in the final mixture ethanol/water was 0.05 M. The corrected temperature rise, due to the stirring heat and the lack of adiabatic conditions, was calculated by the Dickinson method [16].

2.3. Catalytic tests

Conversion tests of GVL to PP in the presence of PL were carried out in liquid phase using a commercial 100 mL autoclave (Parr 4565), equipped with mechanic stirrer.

In a typical experiment, an amount of 1.5 mL GVL (99%, Sigma-Aldrich), 40 mL of PL (pentanol 99%, Sigma-Aldrich), 0.5 mL of hexadecane (99%, Sigma-Aldrich) used as internal standard and 0.25 g of catalyst (calcined *ex-situ*) were charged in inert N_2 atmosphere to the autoclave. In these experiments, PL played both roles, as reactant and solvent and, in these particular conditions, the GVL initial concentration was 0.37 M.

Then, the reactor was heated up to 523 K and the pressure was rapidly increased up to either 10 bar with N_2. This sudden increase of the pressure pushes GVL, initially inside a stainless-steel tube, into the reactor. Thus, any conversion of the GVL during heating stage was avoided. The zero time of reaction was considered when the pressure inside the reactor reached the autogenous pressure plus 10 bar, and the reaction was carried out during 8 h from that initial time. Stirring speeds of 650 rpm and catalyst particle diameters lower than 100 μm were used in order to diminish mass transfer limitations.

Liquid samples were withdrawn from the reactor, every 5–30 min, by using a loop under pressure in order to avoid flushing of volatile components. An Agilent 6850 chromatograph equipped with flame ionization detector (heated at 573 K), temperature programmer, and an HP-1 capillary column (50 m × 0.32 mm ID, 1.05 μm film) was used for monitoring the concentrations of unreacted GVL and reaction products by *ex situ* gas chromatography. The reactant conversion (X_{GVL}, mol of GVL reacted/mol of GVL fed) was calculated as $X_{GVL} = \frac{C^0_{GVL} - C_{GVL}}{C^0_{GVL}} \cdot 100$, where C^0_{GVL} is the initial GVL concentration and C_{GVL} is the GVL concentration at reaction time *t*. Yields (η_j, mol of product j/mol of GVL fed) were calculated as $Y_j = \frac{C_j}{C^0_{GVL}} \cdot 100$, where C_j is the concentration of product j. Selectivities (S_j, mol of product j/mol of GVL reacted) were calculated as $S_j = \frac{C_j}{C^0_{GVL} - C_{GVL}} \cdot 100$. Carbon balance during catalytic runs was estimated as $CB = \frac{C_{GVL} + \sum C_j}{C^0_{GVL}} \cdot 100$, where $\sum C_j$ is the total product concentration in liquid phase. Finally, the missing carbon balance (MCB) was estimated as $MCB = 100 - CB$.

3. Results and discussion

3.1. Characterization results

The amount of ZnO and HPA deposited on ZnO/SiO_2 and HPA/SiO_2, determined by AAS and XRF, were 21.7% and 42.2%, respectively. The X-Ray diffractograms for the samples are shown in Fig. 2. SiO_2 did not show any diffraction signals, in line with the fact that is an amorphous solid. In contrast, the X-Ray diffractogram of γ-Al_2O_3 showed the

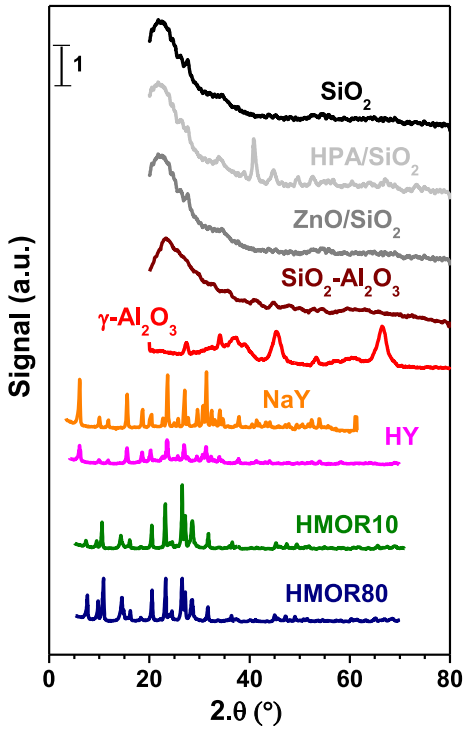

Fig. 2. X-ray diffraction (XRD) patterns of the calcined samples [scan speed. 2°/min].

characteristic signals of the γ crystalline phase, at 2θ = 37.2°, 39.1°, 45.3° and 66.9° (PDF-29-0063). SiO_2-Al_2O_3, similarly to SiO_2, only exhibited an amorphous halo indicating absence of crystalline phases and suggesting that the Al_2O_3 phase is highly dispersed in the SiO_2. Regarding the SiO_2-supported samples, the X-Ray diffractogram of ZnO/SiO_2 exhibited only the amorphous halo of SiO_2 support and did not show any diffraction signals, indicating that the wurtzite phase consists of crystallites smaller than 4 nm. On the other hand, the X-Ray diffractogram of HPA/SiO_2 showed the characteristic diffraction lines of $H_3PW_{12}O_{40}$ with Keggin structure at 2θ = 10.0°, 14.2°, 20.3°, 25.0°, 29.0°, 34.3°, 37.3°, 52.9° and 59.6° (PDF-75-2125). Regarding the zeolites, all the calcined samples showed the characteristic diffraction signals, indicating that the calcination process preserved the structure.

Textural properties of the solids were determined by N_2 physisorption at 77 K and the main results are shown in Fig. 3, whereas the N_2 adsorption/desorption isotherms are presented in Fig. SI 1. The values of the specific surface area of the solids, determined by BET method, are presented in Fig. 3a. All values were in the range 180–700 m^2/g, indicating that in general all these solids exhibited a relatively high specific surface area, a desirable physical property for material to be used as catalyst support. The solid with the lowest value $S_g = 180\ m^2/g$ was γ-Al_2O_3. SiO_2 and SiO_2-supported materials showed S_g values between 205 and 240 m^2/g. The specific surface area of HPA/SiO_2 and ZnO/SiO_2 were 15% and 8% lower, respectively than the value of the SiO_2 support, suggesting a certain pore blockage by precursors after the impregnation processes. Among the non-zeolitic materials, the solid with the highest specific surface area was SiO_2-Al_2O_3 with $S_g = 460\ m^2/g$. In general, specific surface area of zeolitic materials was higher than that of the SiO_2-Al_2O_3 as it can be seen in (Fig. 3). The zeolite with the highest specific surface area was NaY ($S_g = 700\ m^2/g$), followed by the HY ($S_g = 660\ m^2/g$), prepared from the former. In the case of HMOR zeolites, the dealumination process required for obtain the commercial samples HMOR60 and HMOR80 produced an increase in the specific surface area, showing HMOR60 and HMOR80 values of S_g 22% and 30% higher, respectively than the value determined for HMOR10.

In the non-zeolitic samples, the pore volume followed the pattern:

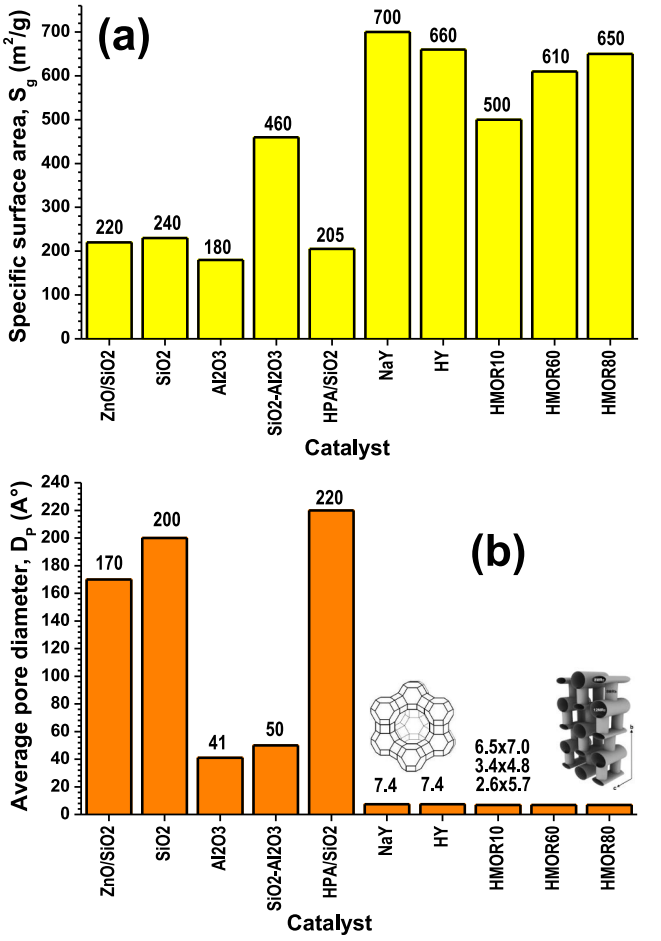

Fig. 3. Textural properties of the calcined samples determined by N_2 physisorption at 77 K. (a) Specific surface area determined by BET method; (b) average pore diameter estimated by BJH method.

SiO_2-Al_2O_3 (0.74 cm^3/g) > HPA/SiO_2 (0.61 cm^3/g) > SiO_2 (0.49 cm^3/g) ≅ ZnO/SiO_2 (0.47 cm^3/g) > γ-Al_2O_3 (0.25 cm^3/g), showing this last sample a pore volume equal to one third of that of SiO_2-Al_2O_3. By using BJH method the mean pore diameter of the non-zeolitic materials was determined, showing that all these samples are mesoporous solids due to, in all the cases, the mean pore diameter was between 2 and 50 nm (Fig. 3b). On the other hand, it is well-known that zeolites are considered microporous solids because the mean pore diameter is lower than 2 nm, and the pore sizes shown in Fig. 3b were taken from literature [17].

Acid density and relative acid strength of calcined samples were probed by temperature-programmed desorption (TPD) of NH_3 preadsorbed at 373 K. The total acid site density was considered as the contribution of: (a) relatively weak acid sites that desorb NH_3 at temperatures lower than 573 K and (b) strong sites that desorb the NH_3 over 573 K. The main results from TPD of NH_3 experiments are shown in Fig. 4, whereas the detailed NH_3 desorption profiles as a function of temperature are presented in Fig. SI 2. The SiO_2 sample did not show NH_3 desorption peaks indicating that it is a non-acidic sample. In contrast, ZnO/SiO_2 showed a broad and intense NH_3 desorption band in the thermal range 493–773 K (maximum at 573 K) indicating the presence of acid sites with a wide variety of strength (weak and strong sites). In the case of HPA/SiO_2 also an intense band was measured, but with two maxima at 475 K and 840 K·NH_3 desorption at T > 773 K reveals the presence of very strong acid sites on the HPA/SiO_2 surface. Diez et al. reported that strong Brønsted acid sites of unsupported HPA desorb NH_3 at about 900 K [18], though other authors reported that the decomposition temperature for HPA is about 740 K [19]. The broad

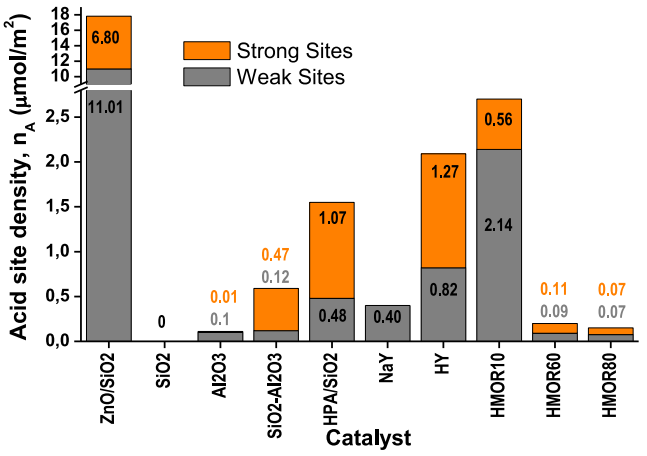

Fig. 4. Acid site density of the calcined samples determined by temperature-programmed desorption (TPD) of NH_3 [heating rate. 10 K/min, flow rate: 60 cm^3/min (He)].

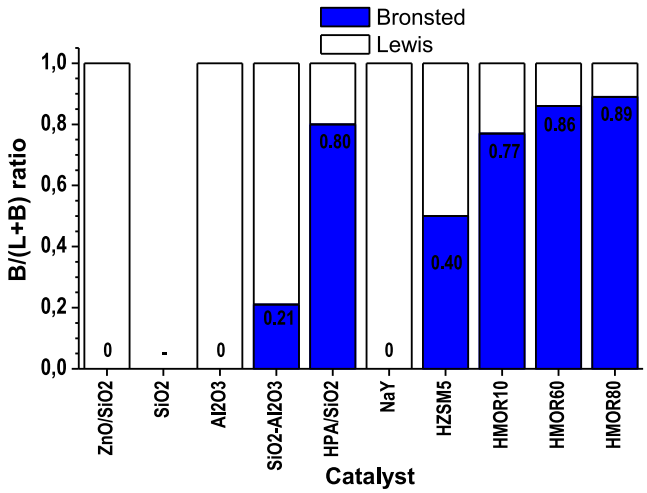

Fig. 5. Brønsted to total acid sites ratio of the calcined samples determined by FTIR of adsorbed pyridine at 298 K and evacuation at 423 K [L. Lewis; B. Brønsted sites].

strength distribution determined for HPA/SiO_2 can be probably the result of the presence of highly support-interacting heteropolyacid species. For the γ-Al_2O_3 sample, only a small NH_3 desorption band with its maximum at 473 K was detected, indicating that only weak acid sites are present on the surface of this solid. In contrast, SiO_2-Al_2O_3 sample showed a broad band between 393 K and 1073 K with its maximum at 517 K and a shoulder at 697 K that strongly suggests the presence of surface sites of different acid strength. Moreover, NH_3 desorption rate diminished as the acid site strength increased.

The NH_3 TPD curves evolved over NaY, HY, and HMOR zeolites are also presented in Fig. SI 2. From the surface of NaY zeolite, NH_3 desorbed in the thermal range 463–663 K, exhibiting an asymmetric band with the maximum at about 505 K, indicating the presence of relatively weak acid sites. In contrast, HY zeolite prepared from NaY by double ion exchange showed the presence of not only weak acid sites, but also strong ones, evidenced by an asymmetric and very broad desorption band between 430 K and 870 K (with its maximum at about 510 K). Finally, the evolved NH_3 from HMOR samples made possible to say that the three samples showed two desorption bands: a low temperature peak between 410 and 630 K assigned to weak acid sites, and a broad high temperature band (650–920 K) that reflects the presence of strong acid sites. However, among these samples the following differences were observed: (i) the surface acid site density of HMOR10 is about one order of magnitude higher than dealuminated HMOR60 and HMOR80 samples; (ii) the position of the maximum is shifted to lower temperatures as the Si/Al ratio increases; (iii) the relative concentration of strong acid sites respect to total acid sites ($n_{A\text{-}HT}/n_A$) is higher for dealuminated samples than for sample HMOR10. These trends are in agreement with the findings of other authors [20,21]. All these results are summarized in Fig. 4, where the proportion of strong acid sites can be compared with the one corresponding to weak ones. From the observation of Fig. 4, it is possible to infer that the samples with an important fraction of strong acid sites in comparison with weak sites are ZnO/SiO_2, SiO_2-Al_2O_3, HPA/SiO_2, HY and HMOR zeolites. Besides, considering the non-zeolitic samples, the surface acid site density (n_a) followed the pattern: ZnO/SiO_2 (17.81 μmol/m^2) > HPA/SiO_2 (1.55 μmol/m^2) > SiO_2-Al_2O_3 (0.59 μmol/m^2) > γ-Al_2O_3 (0.11 μmol/m^2) ≫ SiO_2 (≅ 0 μmol/m^2).

The nature of surface acid sites on the calcined samples was determined by FTIR using pyridine as probe molecule. The FTIR spectra obtained, in the wavenumber range 1400–1700 cm^{-1}, are shown in Fig. SI 3. The IR bands at around 1540 cm^{-1} and 1440–1460 cm^{-1} correspond to pyridine chemisorbed on Brønsted (B) and Lewis (L) sites, respectively [22]. The relative contributions of Lewis and Brønsted acid sites are also presented in Fig. 5.

SiO_2 sample was not tested by FTIR of pyridine due to the fact that it showed no acidity by TPD of NH_3. The FTIR spectrum of ZnO/SiO_2 showed two overlapping absorption bands in the range 1440–1460 cm^{-1} due to pyridine adsorbed on Lewis acid sites. The peak at 1611 cm^{-1} is sensitive to the adsorption mode and provides information on the nature and strength of Lewis acidity, while the peak at 1450 cm^{-1} is characteristic of the number of sites on the surface. The additional bands (1616 and 1450 cm^{-1}) have been explained by other authors based on the nature of the Zn precursor [23] and the effect of residual chlorine, coming from $ZnCl_2$, after calcinations [24]. Indeed, these results indicate that the presence of chlorine generates IR bands at higher frequencies than those corresponding to chlorine-free ZnO. These IR absorption signals are indicative that the strength of the Lewis acidity is increased by the presence of residual chlorine, giving rise to Lewis acid sites with different strength. In the case of HPA/SiO_2 an important band due to pyridine chemisorbed on Brønsted sites was observed with its maximum at 1538 cm^{-1} and a significantly lower band corresponding to pyridine chemisorbed on Lewis sites with the maximum at 1453 cm^{-1}, as well. For HPA/SiO_2, the ratio of Brønsted acid sites respect to total sites was B/(L + B) = 0.80, confirming the presence of mainly Brønsted sites [14]. γ-Al_2O_3 only showed an IR absorption band with the maximum at 1450 cm^{-1} due to chemisorbed pyridine on Lewis acid sites. In contrast, the IR spectra for SiO_2-Al_2O_3 showed not only the pyridine absorption band at around 1545 cm^{-1} characteristic for pyridinium ions adsorbed on Brønsted acid sites, but also the band at 1455 cm^{-1} due to coordinately bound pyridine on Lewis acid sites associated with tricoordinate Al atoms [25]. Thus, the ratio of Brønsted acid sites respect to total sites was B/(L + B) = 0.21 for the SiO_2-Al_2O_3 sample.

Regarding the zeolitic materials, NaY sample exhibited only the band associated to pyridine adsorbed on Lewis acid sites with its maximum at 1444 cm^{-1}. In contrast, HY sample exhibited not only the band for Lewis acid sites (maximum at 1454 cm^{-1}), but also the one for Brønsted sites (maximum at 1543 cm^{-1}), the latter with a lower intensity than the former, leading to a value of B/(L + B) = 0.4. Finally, HMOR zeolites showed both Lewis and Brønsted pyridine adsorption bands at 1453 and 1544 cm^{-1}, respectively. The B/(L + B) ratio of these samples was equal to 0.77, 0.86 and 0.89 for HMOR10, HMOR60 and HMOR80, respectively. In summary, the proportion of Brønsted acid sites to total acid sites followed the pattern (Fig. 5): γ-Al_2O_3 = ZnO/SiO_2 = NaY < SiO_2-Al_2O_3 < HY < HMOR10 < HPA/SiO_2 < HMOR60 < HMOR80.

From all characterization results, it is partially concluded that the density, strength and nature of surface acid sites present in the zeolitic and non-zeolitic materials studied show significant differences. Although for scanning the whole range of B/(L + B) ratio a sample

containing exclusively Brønsted acid sites, such as Amberlyst ion exchange resins, is missing, it is well known that these acid materials are highly unstable at temperatures higher than 423 K [26,27]. Therefore, they cannot be tested in the GVL conversion at 523 K.

3.2. Catalytic results for the conversion of GVL and PL over acid solids

Previously to use of the selected acid solids, a blank test without solid catalyst was performed in order to explore the progress of the reaction in non-catalytic conditions (Table 1). In this test, a GVL conversion of about 5% and HPV yield of about 3% was observed after 8 h, though no PP formation was detected in liquid phase, showing that the presence of acid solid catalyst is required to promote significantly both acid catalysed reactions.

Catalytic conversion of GVL in the presence of PL was performed over the selected acid solids and the results are shown in Fig. 6 and summarised in Table 1. In Fig. 6, not only the X_{GVL} and Y_j vs. t curves obtained during the progress of the reaction are presented, but also the missing carbon balance (MCB) during the run. This MCB was considered as an additional reaction product, although in reality, it represents GVL, GVL-derived intermediate or products strongly adsorbed on the solid surfaced surface.

The GVL conversion on SiO_2, ZnO/SiO_2 and γ-Al_2O_3 was almost constant after 50 min reaction, suggesting a rapid in situ samples deactivation. Thus, X_{GVL} on these solids was lower than 24 % at the end of the 8 h runs. However, only a HPV yield of about 2.9% was detected, without formation of PP or PPV for SiO_2 and ZnO/SiO_2 and a Y_{PP} and Y_{PPV} of 2.1% and 4.3%, respectively for γ-Al_2O_3 (Fig. 6). The qualitative evolution of MCB with time (similar to that of a primary reaction product with positive and different from zero initial slope) suggests that an important fraction of GVL, or intermediate coming from its adsorption, remains strongly adsorbed over the SiO_2, ZnO/SiO_2 and γ-Al_2O_3, even from the beginning of the reaction. Thus, the final MCB was about 20%, indicating that only a minor fraction of the converted GVL was transformed into HPV.

Over HPA/SiO_2 the results were totally different from those observed with SiO_2, γ-Al_2O_3 and ZnO/SiO_2. In this case, HPA/SiO_2 was very active with a final GVL conversion of X_{GVL} = 60.2%, though a remarkable deactivation was observed after 1 h of reaction (Fig. 6). The final Y_{PP} and Y_{PPV} were 25.7% and 4.0%, respectively. The MCB observed over HPA/SiO_2 was some higher than those observed over SiO_2, γ-Al_2O_3 and ZnO/SiO_2, reaching a Y_{MCB} = 29.9% at the end of the run. Besides, the evolution with time of MCB was qualitatively different. From the analysis of low reaction times it is possible to see that the MCB showed a null initial slope of formation, strongly suggesting that these deposits are probably coming from a secondary reaction product. Even more, due to the high ratio PP/PPV in liquid phase observed with this catalyst containing mainly Brønsted acid sites, a high concentration of PP intermediate and PPV in the solid surface is likely the cause of the significant MCB. Besides, an important formation of dipentyl ether was evidenced by GC analysis of liquid-phase samples, indicating that the intermolecular dehydration of pentanol takes place over the strong Brønsted acid sites present in HPA/SiO_2. To investigate the cause of the deactivation of this catalyst, XRF analysis of the spent sample was performed. A W content of 0.6% in the spent catalyst indicated that the HPA loading diminished from 42.2% in the fresh catalyst up to 0.8% after the reaction, evidencing a dramatic leaching process. This is in line with the findings of other authors, who observed a significant leaching of supported HPA in polar solvents [14,28].

SiO_2-Al_2O_3 sample was considerably active for the conversion of GVL and PL into HPV, PP and PPV (Fig. 6), showing an initial GVL conversion rate lower than HPA/SiO_2 but higher than ZnO/SiO_2 and γ-Al_2O_3. The final GVL conversion was X_{GVL} = 58.0% showing a higher production of PP in comparison with PPV, reaching a final Y_{PP} and Y_{PPV} equal to 20.2% and 12.2%, respectively. The HPV yield was maximum at 15 min (Y_{HPV} = 4.3%) and the decreased slowly with time up to a final value of 0.6% at 8 h. The temporal evolution of MCB also indicated that GVL, or intermediates directly coming from the reactant, remain strongly adsorbed on the catalyst surface, reaching a final value of Y_{MCB} = 25.0%. The presence of these strongly adsorbed species on the catalyst surface seem responsible for the almost negligible formation of dipentyl ether from pentanol observed over SiO_2-Al_2O_3. These adsorbed species would block the acidic sites of the support, preventing the etherification of pentanol.

Regarding the zeolitic materials, catalytic results obtained over NaY zeolite were similar to those obtained with ZnO/SiO_2 and γ-Al_2O_3.

HY zeolite exhibited a much higher initial GVL conversion rate than NaY, reaching a X_{GVL} = 55.0% at the end of the run (Fig. 6). Although the evolution of GVL conversion and Y_{HPV} were quite similar than those observed over SiO_2-Al_2O_3 catalyst, the formation rates of PP and PPV were significantly higher, reaching final values of Y_{PP} = 32.2% and Y_{PPV} = 14.5% over HY. In contrast with SiO_2-Al_2O_3 catalyst, the MCB followed a completely different temporal evolution over HY, because the initial slope of the Y_{MCB} was null, indicating that the MCB on HY sample comes from the strong adsorption of a secondary reaction product (PP or PPV). The final MCB with HY after 8 h of reaction was equal to 8.3%, one third of the value observed over SiO_2-Al_2O_3 with a similar final X_{GVL} conversion. On the other hand, it is relevant to mention that during the whole run an important rise in the total pressure inside the reactor was

Table 1
Summary of catalytic activity results obtained over the acid solids.

Sample	X_{GVL} = 20%				X_{GVL} = 50%				End of reaction					
	Y_{HPV}[a] (%)	Y_{PP}[a] (%)	Y_{PPV}[b] (%)	MCB[c] (%)	Y_{HPV}[a] (%)	Y_{PP} (%)	Y_{PPV} (%)	MCB (%)	Time (min)	X_{GVL}[d] (%)	Y_{HPV}[a] (%)	Y_{PP} (%)	Y_{PPV} (%)	MCB (%)
Blank	–	–	–	–	–	–	–	–	480	5	3	0	0	2
SiO_2	2.0	0	0	18.0	–	–	–	–	480	23.0	2.9	0	0	20.1
ZnO/SiO_2	2.4	0	0.2	17.2	–	–	–	–	480	21.8	2.8	0	0.8	18.2
HPA/SiO_2	0.9	17.0	2.1	0	0.9	25.5	3.3	20.3	480	60.2	0.6	25.7	4.0	29.9
γ-Al_2O_3	5.6	0.5	0.9	13.0	–	–	–	–	480	22.1	2.9	2.1	4.3	12.8
SiO_2-Al_2O_3	4.3	1.0	0.6	14.1	2.1	12.2	8.9	26.8	480	58.0	0.6	20.2	12.2	25.0
NaY	–	–	–	–	–	–	–	–	480	15.5	2.4	3.8	1.1	8.2
HY	3.3	12.1	4.1	0.5	0	31.4	13.6	5.0	480	55.0	0	32.2	14.5	8.3
HMOR10	3.9	2.2	4.8	9.1	–	–	–	–	480	22.7	3.2	2.8	6.4	10.3
HMOR60	1.8	2.8	8.6	6.8	1.4	10.4	21.6	16.6	480	64.2	1.1	26.0	20.5	16.6
HMOR80	1.3	4.3	14.2	0.2	1.4	17.0	24.6	7.0	180	55.8	1.2	30.0	24.4	0.2

Y_{PP}: molar yield to pentyl 2-pentenoate.
Y_{PPV}: molar yield to 4-pentoxy pentyl valerate.
MCB: missing carbon balance.
X_{GVL}: γ-valerolactone conversion.

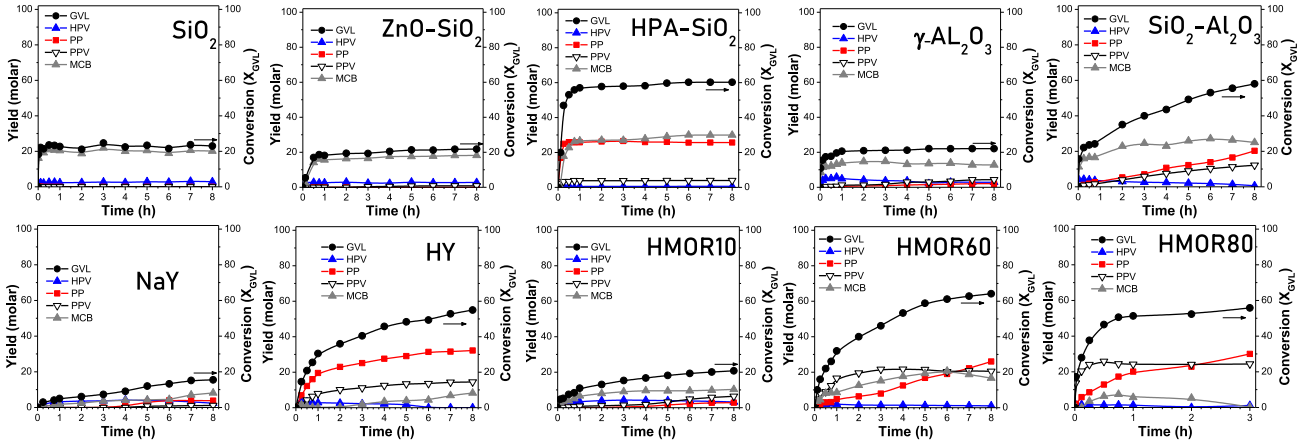

Fig. 6. Catalytic activity results for the conversion of GVL in the presence of PL over the calcined samples [T = 523 K, p = 10 bar (N_2), W_C = 0.25 g, V_{PL} = 40 mL, C^0_{GVL} = 0.37 M, stirring rate = 650 rpm].

evidenced, suggesting a significant production of gaseous product over HY zeolite. A GC analysis of the gas phase inside the reactor indicated that the main components were pentene isomers, by-products coming from the dehydration of PL solvent. Besides, a relatively high amount of dipentyl ether was detected by GC in the liquid phase, indicating that the undesirable intermolecular dehydration of pentanol also takes place over HY zeolite.

The HMOR10 zeolite sample showed a catalytic performance similar to that of the NaY zeolite, though the activity was slightly higher, reaching a final GVL conversion of 22.7% after 8 h (Fig. 6). The final yields of these secondary products were Y_{PP} = 2.8% and Y_{PPV} = 6.4%. The MCB exhibited a primary product-like behaviour with a maximum value at the end of the run of Y_{MCB} = 10.3%. No increase of the total pressure inside the reactor was observed with HMOR10, though dipentyl ether formation was detected.

On the other hand, HMOR60 zeolite, with a higher Si/Al ratio, was significantly more active than HMOR10, with a larger production of secondary products PP and PPV (Fig. 6). PPV reached a maximum yield Y_{PPV} = 21.7% and was almost constant after 3 h reaction. In contrast, PP yield constantly increased with time, up to a final value after 8 h of Y_{PP} = 26.0%. It is worth noticing that MCB, though initially behaved as a primary reaction product reached a maximum yield of Y_{MCB} = 20.7% at 6 h and then decreased up to a final value Y_{MCB} = 16.6% at 8 h. This particular evolution of MCB suggests that at high GVL conversion levels (X_{GVL} > 60%) the surface intermediates coming from GVL adsorption can be converted mainly into PP, at the light that Y_{PP} increases with time and Y_{PPV} remains constant after 3 h. As in the case of HY, over this zeolite, a significant rise in the total pressure inside the reactor was observed, indicating an important formation of pentene from PL. Besides a high concentration of dipentyl ether was observed in liquid phase, similar to than over HY zeolite, and much higher than over HMOR10.

Finally, HMOR80 zeolite was in line with those observed with HMOR60. However, the intramolecular pentanol dehydration was so important that the reactor pressure increased over 30 bar after 3 h. This dramatic pentene formation made impossible to continue the experiment due to safety conditions and the run had to be stopped at 3 h (Fig. 6). In spite of this shorter reaction time, a final GVL conversion of 55.8% was reached. The evolutions with time of HPV, PP, PPV and MCB yields were similar to those over HMOR60. The MCB followed a primary product-like evolution reaching a maximum value of 7.4% but then dropped becoming almost null at 3 h.

At the light of remarkable differences in catalytic behaviour of the acid solids and the wide range of textural properties, density, strength and nature of acid sites, it is hard to correlate all the experimental observations.

Regarding of textural properties (pore structure) and catalytic tests results it is clear that all reaction products HPV, PP and PPV were formed on the microporous samples (HY and HMOR) as well as mesoporous ones (HPA/SiO_2 and SiO_2-Al_2O_3). These results indicate that the shape selectivity does not play an important role in the catalytic behaviour of these acid solids. Nevertheless, some clear tendencies regarding acid properties and catalytic activity can be underlined.

Acid solids containing exclusively Lewis sites such as γ-Al_2O_3, ZnO/SiO_2 or with no appreciable acidity (SiO_2) show low GVL conversion (<24%). A remarkable missing carbon balance (MCB) is observed (Fig. 6), indicating that GVL and/or a surface intermediate coming from GVL remain strongly adsorbed on the solid surface. This was also observed with NaY zeolite. These results strongly suggest that neither weak Lewis acid sites in γ-Al_2O_3 and NaY nor strong Lewis sites in ZnO/SiO_2 do promote the nucleophilic addition of the PL to the carboxylic group of GVL. Nevertheless, the Lewis acid sites favored the strong adsorption of GVL and may explain the significant deactivation observed for these catalysts. On the other hand, the catalytic behaviour was not strongly affected neither by the acid site density nor by the acid strength, at the light that neither the low acid site density of γ-Al_2O_3 nor the very high acid site density of ZnO/SiO_2 (involving weak and strong acid sites) were efficient to promote the GVL conversion into HPV, PP and PPV. For these samples, the conversion of pentanol into pentenes and/or dipentyl ether was not observed.

SiO_2-Al_2O_3, containing acid sites of wide strength and about 20% of Brønsted nature, was considerably active reaching a X_{GVL} = 58% after 8 h. Although the significant MCB on this sample also seems to come from GVL adsorption, at high reaction times (or X_{GVL} > 50%), MCB started to decrease as PP and PPV formation becomes important (Fig. 6). It is likely that Brønsted acid sites initially covered by GVL (at low X_{GVL} levels), at high X_{GVL} levels become available for HPV dehydration into PP or conversion to PPV with PL. This is in agreement with the good results obtained over bifunctional catalysts for this reaction where SiO_2-Al_2O_3 was used as support [11,12]. Even more, when a metal phase is deposited on this support and H_2 is present in the reaction media, relatively high PV yield is achieved and the CB is much closer to 100%, strongly suggesting that the MCB is due to PP strongly adsorbed on acid sites. In this sense, though the catalytic performance of SiO_2-Al_2O_3 in the absence of H_2 and metal phase seems to be discrete, the picture seems to be different when the one-pot process is carried out with H_2 and SiO_2-Al_2O_3-supported bifunctional catalysts.

If the proportion of Brønsted sites is relatively high, as in the case of HPA/SiO_2, the apparent GVL conversion is faster than over SiO_2-Al_2O_3 and a more significant production of PP intermediate is produced in comparison with the undesirable PPV (Fig. 6). Although a relatively high MCB was observed over HPA/SiO_2 and its formation is more likely to happen from a secondary reaction product such as PP and mainly PPV,

the remarkable leaching process seems to be the reason for the dramatic deactivation. Finally, over HPA/SiO_2 a significant formation of dipentyl ether takes place, indicating that Brønsted acid sites are very active not only for the desirable PP formation, but also for the undesirable etherification of pentanol.

The GVL conversion rate with HY zeolite was very similar than that observed with SiO_2-Al_2O_3 (Fig. 6), though the product distribution and evolution was totally different. In contrast to SiO_2-Al_2O_3, HY has a relatively high density of strong and weak acid sites and a higher proportion of Brønsted sites; and this make a remarkable difference in the formation of PP and PPV and the MCB behaviour. Over HY the MCB followed an evolution with time similar than that of a secondary reaction product. An advantage of using HY as acid support is the fact that PP formation was remarkedly higher than PPV. Nevertheless, this zeolite was also very active not only for dehydrating intramolecular PL into pentenes increasing markedly the pressure inside the reactor, but also for converting pentanol into dipentyl ether by intermolecular dehydration. The progress of the former undesirable reaction is a clear disadvantage of HY because the conversion of PL into pentenes reduce the concentration of PL in liquid phase and increases the probability of deactivation of acid sites by strong olefin adsorption. This drawback hampers the use of HY as acid support for bifunctional catalysts to be used this reaction (ROUTE 2, Fig. 1). However, this support was employed by Yan et al. [29], along the ROUTE 1. Particularly, they studied PV and pentane production from GVL over Pd (5%)/HY without using pentanol because the reaction path involved in the PV production was based in ROUTE 1 (Fig. 1), though the use of octane as solvent was reported.

In the case of HMOR zeolites, the effect of Si/Al ratio, the total acid site density, and the B/(L + B) ratio on the selectivity at $X_{GVL} = 20\%$ was analysed. Dealumination process, leading to a higher Si/Al ratio in HMOR zeolites, diminished markedly the total acid site density n_A (Fig. 4) and increased slightly the proportion of Brønsted acid sites (Fig. 5). It is observed that the lower the total acid site density and the higher proportion of Brønsted acid sites (HMOR60 and HMOR80, Figs. 4-5, the higher the selectivity to PP and PPV and reduce the MCB (Table 1). However, the dehydration of PL into pentene was significant over these zeolites and a high concentration of dipentyl ether was observed for HMOR60. Even more, for HMOR80 sample the catalytic run must be stopped after 3 h due to the high concentration of pentenes, which caused the deactivation of the catalyst as well as the dramatic boost in the reactor pressure (Fig. 6). For these reasons, HMOR zeolites cannot be considered an efficient acid support for bifunctional catalysts.

All the previously discussed results allow to affirm that SiO_2-Al_2O_3, containing both Lewis and Brønsted acid sites of wide strength, can be a suitable acid support for bifunctional catalysts for this process due to: a) considerable activity in GVL conversion to PP even after 8 h; b) negligible formation of gas by-products coming from PL dehydration; c) appreciable stability in this reaction conditions. This is in line with the previously reported successful use of this solid in combination with a metal phase to desorb the significant amount of PP adsorbed on acid sites by the action of H_2, leading to the desirable PV production [11,12].

In the case of the SiO_2-Al_2O_3 tested, the composition of this amorphous material is about 90% SiO_2 (in fact 89.2% based on Si/Al = 7), and the aluminum has been incorporated in the SiO_2 during the manufacturing process. In silico-aluminates with this composition, an important amount of penta and tetracoordinated aluminum has been observed by different characterization techniques [30], with a small fraction of HO-groups is in the neighbourhood of Al atoms, whereas the majority of Brønsted acid sites are silanol groups located quite far from the Al atoms. In this sense, Crépeau et al. pointed out that HO– on SiO_2-Al_2O_3 can be classified into two groups: (a) silanol groups as the ones present in pure SiO_2 and (b) hydroxyl groups attached to Si atoms but in the vicinity of Al atoms [30]. Thus, the acidity of SiO_2-Al_2O_3 is quite complex at the light of the different species present, Lewis acid sites coming from the presence of Al atoms in the SiO_2 network and Brønsted acid sites, mainly Si-OH groups, which strength can be strongly influenced by the distance from Al atoms. In this sense, Si-OH, Al(IV) paired sites, according to the literature, seem to be the strongest acid sites. However, the proximity to Al atoms is a continuous function, so a wide range for the acid strength of Brønsted acid sites is expected.

With the aim of getting a deeper insight on the interaction of GVL and PL with the acid sites on SiO_2-Al_2O_3, additional studies involving temperature programmed desorption and oxidation of GVL and PL and calorimetric adsorption studies were carried out over this selected solid.

3.3. Calorimetric determination of adsorption enthalpies of GVL and PL combined with temperature programmed oxidation (TPO) over SiO_2-Al_2O_3

The average molar adsorption enthalpies (ΔH, kcal.mol^{-1}) of GVL and PL over SiO_2-Al_2O_3 sample were determined by calorimetry combined with temperature programmed oxidation experiment (TPO) of the spent samples after the calorimetric tests.

The thermograms observed during the calorimetric tests are presented in Fig. 7a–b for GVL and PL, respectively. Applying Dickinson's method was possible to estimate an extensive adsorption enthalpy of 29.9 cal for GVL and 17.4 cal for PL. In order to obtain intensive values of the adsorption enthalpy for the reactants, the amount of carbon deposited on these samples during the calorimetric tests was determined by TPO. The TPO profiles determined for GVL and PL are shown in

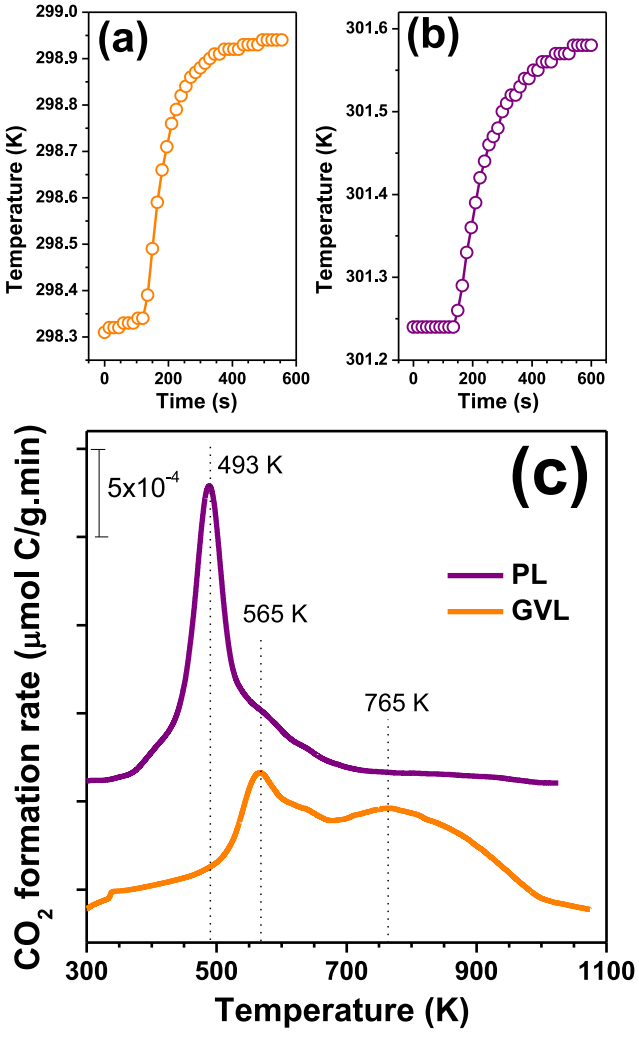

Fig. 7. Calorimetric adsorption results with (a) GVL and (b) PL and (c) temperature-programmed oxidation (TPO) results of GVL and PL adsorbed on SiO_2-Al_2O_3 [O_2(2%)/N_2 stream with a heating rate of 10 K min^{-1}].

Fig. 7c. In the case of adsorbed PL, a single and relatively narrow oxidation band was observed, with its maximum at 493 K. In contrast, the oxidation of adsorbed GVL took place in a wider range of temperature, showing a maximum at 565 K and 765 K. Taking into account that the amount of C deposited during the GVL and PL adsorptions was 56.4 μmol and 23.5 μmol and the stoichiometry coefficient between moles of C and moles of GVL and PL is 5, then the intensive adsorption enthalpies for GVL and PL are 61.9 Kcal.mol^{-1} and 59.1 Kcal.mol^{-1}. These relatively high values reflect a strong GVL and PL adsorption over the acid sites in the surface of SiO_2-Al_2O_3, in agreement with the findings of other authors also using SiO_2-Al_2O_3 [6] and others with silico-aluminate materials [31]. In this last case, Novodárszki et al. observed the formation of strong hydrogen bonds between GVL and Brønsted acid sites hydroxyl groups in the protonic form of aluminum-containing magadiite (HMAG) [31]. The FTIR results of these authors strongly suggested that both silanol and strong Brønsted acid hydroxyl groups are involved in the adsorption of GVL over HMAG, what can explain the relatively high enthalpy of GVL adsorption determined in this work. Although these authors studied the hydroconversion of GVL into pentanoic acid without the presence of PL, they agreed with the fact that ring opening provided most probably pentenoic acid intermediate that was the saturated by the action of H_2. In contrast in our case, though the interaction and strong adsorption of GVL with Brønsted acid sites could be very similar, the presence of adsorbed pentanol modifies completely the reaction scheme, forming as primary reaction product HPV instead of pentenoic acid.

3.4. Temperature programmed desorption of GVL and PL from SiO_2-Al_2O_3

The strength and reversibility of the GVL/SiO_2-Al_2O_3 and PL/SiO_2-Al_2O_3 interaction were studied by temperature-programmed desorption (TPD) and the results are presented in Fig. 8. In these tests, desorption temperature of the pre-adsorbed molecule (GVL or PL) was taken as a measure of the strength of adsorption over the acid sites. When the reactant is not desorbed as the original molecule, fragments coming out from its decomposition were detected, indicating that the reactant adsorption over the acid sites was very strong and irreversible.

The main fragments with their relative abundance observed in the mass spectrum of GVL taken as reference (Fig. SI 4a) are m/z = 56 (100%), 85 (48%), 41 (47%) and 43 (30%). The results obtained in the TPD experiments with GVL are shown in Fig. 8a. A single desorption peak with its maximum at 593 K was detected, characterized by the evolution of fragments m/z = 41, 39, 27 and 56. Simultaneously to these fragments, a relatively intense fragment m/z = 44 was observed. Fragments with m/z = 85 and 43 were not observed and the fragment m/z = 56 was not the most abundant signal. These results indicate that GVL chemisorbs irreversibly and very strongly over acid sites on SiO_2-Al_2O_3. The evolved fragments are in agreement with the decomposition of strongly adsorbed GVL into butene and CO_2, products coming from the GVL decarboxylation. The fragments shown in Fig. 8a are in line with the reference spectra of 1-butene and CO_2 (Fig. SI 4b and SI 4c, respectively). This reaction has been previously reported over SiO_2-Al_2O_3 for obtaining butene by other authors [6]. This irreversible strong adsorption of GVL can explain the significant MCB observed during the liquid-phase reaction with PL (Fig. 6).

On the other hand, the main fragments of the mass spectrum of PL according to literature are m/z = 42 (100%), 55 (96%), 41 (70%), 70 (50%), 29 (35%) and 27 (20%) (Fig. SI 4d). The evolved fragments detected during the TPD of PL are shown in Fig. 8b. A single desorption peak with its maximum at 478 K was observed, characterized by the evolution of fragments m/z = 55, 42, 29, 27, 41 and 70. Simultaneously to these fragments, a relatively intense signal corresponding to fragment m/z = 18 was observed, indicating the evolution of water. Though the relative intensities of the observed fragments are not very different from that of the reference PL spectrum, the simultaneous evolution of water strongly suggests dehydration of PL over acid sites. This dehydration could be both intramolecular leading to 1-pentene and intermolecular to dipentyl ether, as other authors observed over Al_2O_3 in temperature programmed desorption of PL [32]. The main fragments of 1-pentene according to literature are m/z = 42 (100%), 55 (66%), 41 (44%), 70

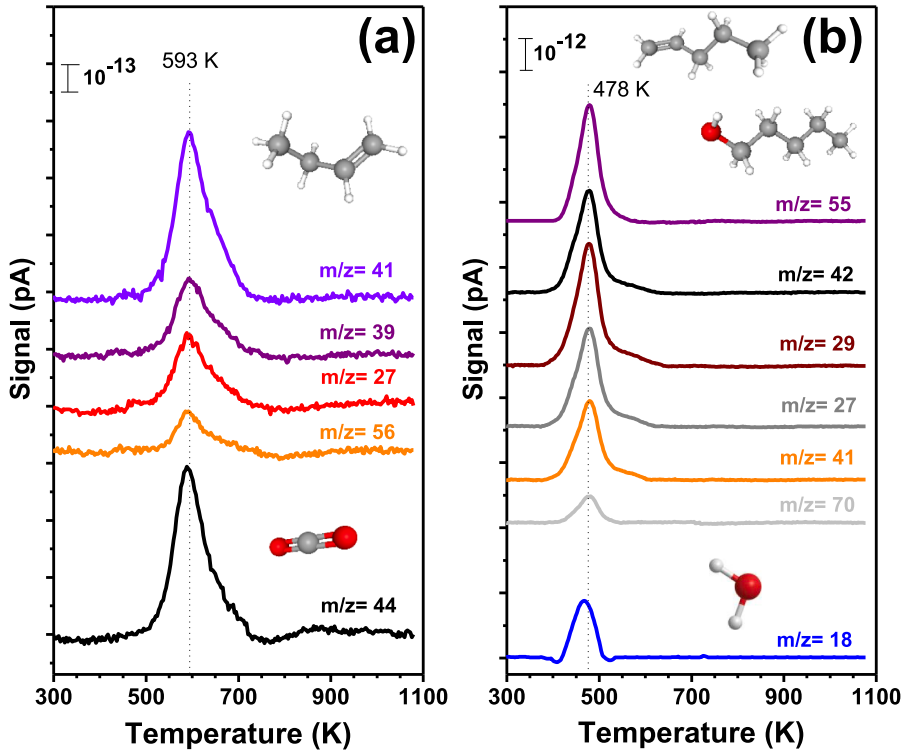

Fig. 8. Temperature-programmed desorption (TPD) profiles of: (a) GVL and (b) PL adsorbed at room temperature over SiO_2-Al_2O_3. [heating rate. 10 K/min, flow rate. 60 cm^3/min (He)].

(40%) and 39 (28%) and for dipentyl ether are $m/z = 71$ (100%), 43 (84%), 70 (42%), 41 (18%) and 69 (18%) (Fig. SI 4e and SI.4.f, respectively). Although some fragments matched with the ones detected, the main fragments for dipentyl ether $m/z = 71$ and $m/z = 43$ were not detected in the TPD experiment. This could be a consequence of a deeper fragmentation of these fragments into smaller ones, so the desorption of PL as dipentyl ether cannot be disregarded. On the other hand, the detected fragments matched well with the main fragments of PL and 1-pentene, indicating that intramolecular dehydration of adsorbed PL into 1-pentene actually takes place, though a fraction of PL desorbs as itself. In other words, PL adsorbs relatively strongly over SiO_2-Al_2O_3 and both reversibly and irreversibly, desorbing as PL and 1-pentene, respectively, and probably as dipentyl ether as well.

It is worth noticing that both decomposition of adsorbed GVL and PL observed during the TPD experiments occurs at temperatures higher than the liquid-phase reaction, in agreement with the fact that the pressure inside the reactor did not increase by the formation of butene and pentene when SiO_2-Al_2O_3 was tested as catalyst at 523 K.

In summary, the TPD experiment showed that: (1) Both GVL and PL adsorption over SiO_2-Al_2O_3 are very strong; (2) GVL adsorbs slightly stronger than PL over acid sites on SiO_2-Al_2O_3; (3) The adsorption of GVL is irreversible leading to decarboxylation to butene; (4) The PL adsorption is both reversible and irreversible, with dehydration of PL into 1-pentene and dipentyl ether.

3.5. Effect of the calcination temperature on the catalytic performance of SiO_2-Al_2O_3

Finally, the effect of the calcination temperature on the catalytic performance of SiO_2-Al_2O_3 was evaluated by calcining at 873 K by 2 h. It is well-known that increasing the calcination temperature in aluminosilicates leads to a reduction of acid site density and an increase of the L/(L + B) ratio, due to dehydroxilation [33,30]. The differences in the TPD of NH_3 profiles for SiO_2-Al_2O_3 calcined at 773 K and 873 K are shown in Fig. SI 5. The total acid site density n_A diminished about 10% (from n_A = 0.59 μmol/m^2 up to 0.54 μmol/m^2) and the temperature of the maximum desorption rate shifted 50 K to higher temperatures (from 523 K up to 573 K). Besides, the shoulder at 703 K exhibited by the sample calcined at 773 disappeared when the calcination was performed at 873 K. The catalytic performance of SiO_2-Al_2O_3 calcined at 773 K and 873 K is compared in Fig. 9 and important differences can be observed. The sample calcined at 873 K was initially slightly less active and showed a higher formation rate of PP and PPV in comparison with MCB. Besides, after 8 h a Y_{PP} = 11.5% and Y_{PPV} = 17.8% were reached, indicating that with a lower acid site density and higher Lewis acid site proportion, the PPV formation is more favoured than the HPV intramolecular dehydration into PP. This could be due to a more important PL adsorption over Lewis acid sites than GVL adsorption. Even more, the temporal evolution of MCB was totally different when the sample was calcined at 873 K, suggesting that this harder calcination reduces the density of active sites than keep intermediates or GVL strongly adsorbed. Thus, the MCB evolution was similar than that of a secondary reaction product, in contrast with the primary behaviour showed at lower calcination temperature (Fig. 9). Although this seems a positive change, over SiO_2-Al_2O_3 calcined at 873 K after 8 h the MCB reached a value of 40.6%, a significantly higher value than 25% observed with the milder calcination.

In summary, a calcination temperature of 773 K for SiO_2-Al_2O_3 is more appropriate for a higher PP formation over PPV, though a relatively high MCB is observed at the beginning of the process due to a stronger GVL adsorption. Nevertheless, if the SiO_2-Al_2O_3 is used as acid support of a metal phase deposited by impregnation [11,12] taking part in a M/SiO_2-Al_2O_3 bifunctional catalyst, the simultaneous presence of a metal function and dissociatively chemisorbed H favors the consumption of PP intermediate, pulling the equilibrium GVL + PL ↔ HPV → PP + H_2O toward products during the one-pot reaction leading to PV formation.

The findings of this work related to the role of acid sites in the complex conversion of GVL with PL to produce PV biofuel in an one-pot process are relevant for the future design of more efficient bifunctional catalysts, where not only the metal dispersion, but also the density, strength and nature of acid sites should be accurately tuned.

3.6. Validation of results for the pentyl valerate production over bifunctional catalysts

Finally, with the aim of confirming the selection of SiO_2-Al_2O_3 as an efficient support, additional experiments of PV production from GVL, PL and H_2 in the presence of bifunctional catalysts were carried out. In these experiments bifunctional catalysts based on Pt (with a metal loading of about 1%wt) and supported on HY zeolite and SiO_2-Al_2O_3 were employed. Specific details regarding preparation and catalytic tests are given in section SI.4 of Supporting Information.

In agreement with the results over the bare support, Pt/HY catalyst seemed to be an efficient catalyst for the PV production. The catalytic activity results over this bifunctional catalyst are shown in Fig. 10. A

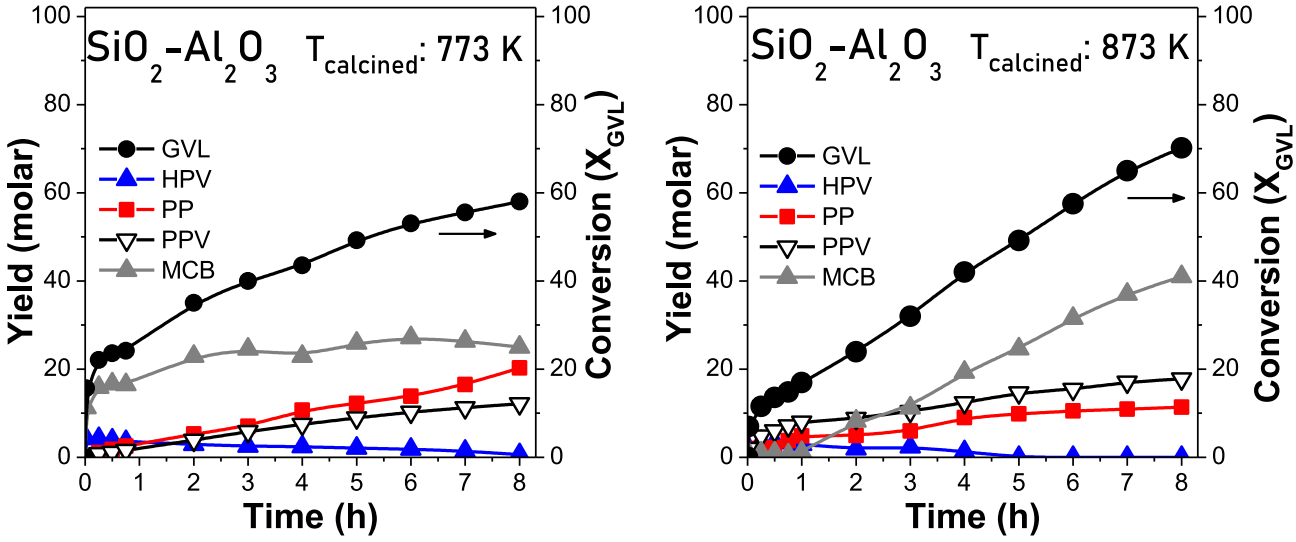

Fig. 9. Catalytic activity results for the conversion of GVL in the presence of PL over SiO_2-Al_2O_3 calcined at 773 K and 873 K [T = 523 K, p = 10 bar (N_2), W_C = 0.25 g, V_{PL} = 40 mL, C^0_{GVL} = 0.37 M, stirring rate = 650 rpm].

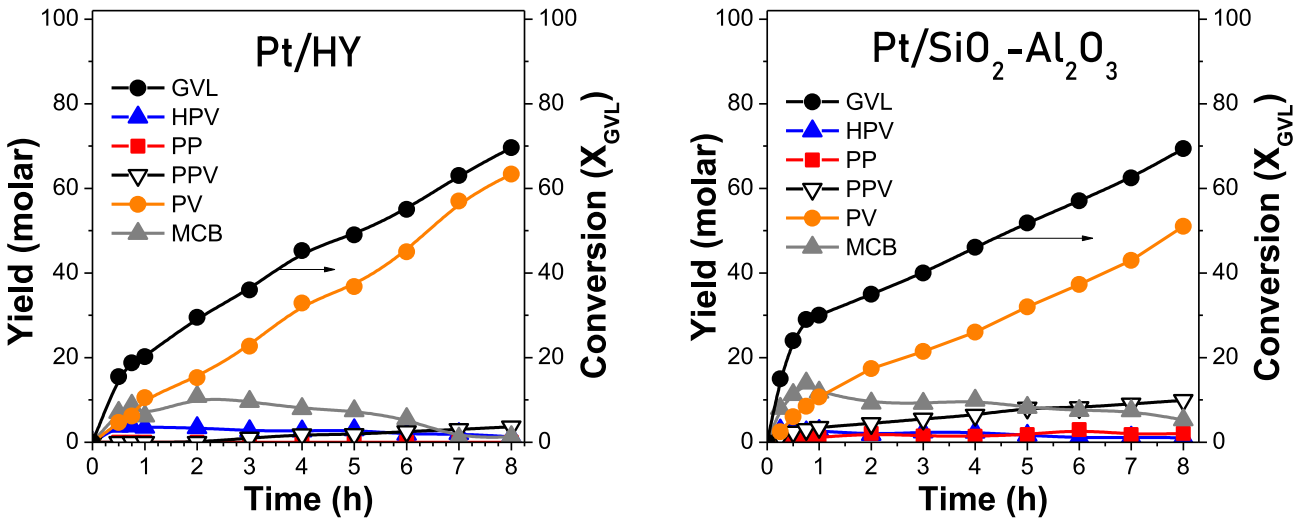

Fig. 10. Catalytic activity results for the production of PV from GVL, PL and H_2 over Pt/HY and Pt/SiO_2-Al_2O_3 bifunctional catalysts [T = 523 K, p = 10 bar (H_2), W_C = 0.25 g, V_{PL} = 40 mL, C^0_{GVL} = 0.37 M, stirring rate = 650 rpm].

final GVL conversion 69.6% and a PV yield of 63.4% were reached, showing a very high PV selectivity. The final yield of HPV, PP and PPV was 1.3, 0 and 3.6%, respectively, whereas the MCB after 8 h reached 1.3%. Nevertheless, the incorporation of Pt onto the HY support did not prevent the pentene and dipentyl ether formation from PL. In other words, an undesirable important increase in the total pressure was evidenced during the reaction and undesirable reaction products coming from PL dehydration in the reaction mixture, as well.

Finally, the catalytic performance of Pt/SiO_2-Al_2O_3 sample is also presented in Fig. 10. After 8 h a GVL conversion of 69.4% and a PV yield of 51.0% were obtained, i.e. a selectivity slightly lower than in the case of HY. The final yield value of HPV, PP and PPV was 1.1, 2.1 and 1.3%, respectively. Besides, the MCB was 5.3%, a considerably lower value than for the SiO_2-Al_2O_3 support. Furthermore, this bifunctional catalyst behaved similarly to the bare support regarding the undesirable PL dehydration; i.e. no formation of dipentyl ether and/or pentene was verified during the reaction.

In summary, from catalytic activity results over bifunctional samples, it can be said that:

1) The GVL conversion is some higher with the bifunctional catalysts than with the acid supports. This confirms that the consumption of PP by hydrogenation to PV pulls the equilibrium of the consecutive acid-catalysed reactions: GVL + PL ↔ HPV ↔ PP + H_2O, reaching a higher GVL conversion after 8 h with bifunctional catalysts.
2) The PP yield is considerably lower over the bifunctional catalysts than over the acid supports, due to the promotion of the hydrogenation reaction by the presence of Pt^0 and 10 bar of H_2.
3) The missing carbon balance (MCB) is lower with the bifunctional catalysts than with the acid supports, confirming the fact that the simultaneous presence of a metal function and chemisorbed hydrogen promotes the hydrogenation of PP adsorbed on the catalyst surface. These results are suggesting that most of the MCB is due to PP adsorbed on the catalyst surface.
4) The PPV yield was lower with the bifunctional samples than over the bare supports, suggesting that the presence of the metal function and chemisorbed hydrogen also modified the progress of the undesirable acid-catalysed reaction: HPV + PL ↔ PPV + H_2O. In this sense the presence of the metal particles on the support surface seems to modify the adsorption of PL, reducing the surface concentration of this reactant.

4. Conclusions

The one-pot conversion of γ-valerolactone to pentyl valerate biofuel in the presence of pentanol and H_2 requires an efficient support selection for the bifunctional catalyst. The acid support plays a key role in the global catalytic performance because the first two reactions of the one-pot process are acid-catalysed reactions.

Solids with no acidity (SiO_2) or with exclusively Lewis acidity (γ-Al_2O_3 and ZnO/SiO_2) and with wide different acid site density showed a non-satisfactory catalytic performance, even zeolites such as NaY.

In contrast, catalyst based on mainly Brønsted acid sites (HPA/SiO_2) was initially very active for converting γ-valerolactone into mainly pentyl 2-pentenoate and in a minor degree 4-pentoxy pentyl valerate. However, HPA/SiO_2 presented a dramatic deactivation cause by a severe leaching process in the polar reaction medium.

HY zeolite containing between 40% of Brønsted acid sites was very active in the conversion of γ-valerolactone to mainly pentyl 2-pentenoate and 4-pentoxy pentyl valerate, however the pentanol dehydration also takes in a significant degree. This behavior is also observed over zeolites with a proportion of Brønsted acid sites between 86 and 89% (HMOR), becoming this problem more serious as the Si/Al ratio increases.

Finally, mesoporous SiO_2-Al_2O_3 with a B/(L + B) ratio of 0.21 and a wide acid site density, proved to be very active showing a selectivity to pentyl 2-pentenoate higher than to 4-pentoxy pentyl valerate. Furthermore, the pentanol dehydration did not take place. On the other hand, this catalyst showed a high missing carbon balance, however these deposits on the catalyst surface can be easily removed when a metal phase and H_2 are present in the system, confirming that SiO_2-Al_2O_3 is an appropriate support for bifunctional catalysts by promoting the conversion of γ-valerolactone into pentyl 2-pentenoate.

Over SiO_2-Al_2O_3 a very strong reactant adsorption was determined. Besides, this adsorption of γ-valerolactone proved to have an irreversible character, whereas in the case of pentanol is partly reversible. Finally, an increase in calcination temperature reduced significantly the ratio PP/PPV and modifying the evolution with time of the missing carbon balance. This confirms that stronger Lewis acid site formed by dehydroxilation of surface silanol groups seem to adsorb pentanol in a higher degree than γ-valerolactone.

An adequate Lewis/Brønsted balance, acid strength and acid site density are responsible for a major production of the relevant intermediate pentyl 2-pentenoate, instead of the undesirable 4-pentoxy pentyl

valerate. Finally, strongly adsorbed intermediates observed with catalysts containing Brønsted acid sites seem to be easily removed when a metal phase and H_2 are present in the system.

CRediT authorship contribution statement

Karla G. Martínez Figueredo: Conceptualization, Validation, Formal analysis, Investigation, Resources, Writing – review & editing. **Darío J. Segobia:** Conceptualization, Methodology, Formal analysis, Writing – review & editing, Visualization, Supervision. **Nicolás M. Bertero:** Conceptualization, Methodology, Resources, Writing – original draft, Writing – review & editing, Visualization, Supervision, Project administration, Funding acquisition.

Declaration of Competing Interest

The authors declare the following financial interests/personal relationships which may be considered as potential competing interests: Nicolas Maximiliano Bertero reports financial support was provided by Agencia Nacional de Promoción Científica y Tecnológica. Nicolas M. Bertero reports financial support was provided by Universidad Nacional del Litoral. Nicolas M. Bertero reports financial support was provided by Consejo Nacional de Investigaciones Científicas y Técnicas.

Acknowledgements

The authors thank Universidad Nacional del Litoral (Grant CAID-2020-50620190100066LI), Consejo Nacional de Investigaciones Científicas y Técnicas (Grant PIP 2015-767), and Agencia Nacional de Promoción Científica y Tecnológica (Grant PICT-2015-3545 from ANPCyT) from Argentina, for the financial support.

Appendix A. Supplementary data

Supplementary data to this article can be found online at https://doi.org/10.1016/j.ecmx.2021.100162.

References

[1] Conti J, Holtberg P, Doman LE, Smith KA, Vincent KR, Barden JL. World Energy Outlook 2011. Energy Information Administration 2011.
[2] Babb BA, Pruett MK. April 2021;57(2):2021.
[3] Zinoviev S, et al. Next-generation biofuels: Survey of emerging technologies and sustainability issues. ChemSusChem 2010;3(10):1106–33. https://doi.org/10.1002/cssc.201000052.
[4] Yan K, Yang Y, Chai J, Lu Y. Catalytic reactions of gamma-valerolactone: A platform to fuels and value-added chemicals. Appl Catal B Environ 2015;179:292–304. https://doi.org/10.1016/j.apcatb.2015.04.030.
[5] Bond JQ, Martin Alonso D, West RM, Dumesic JA. γ-Valerolactone Ring-Opening and Decarboxylation over SiO2/Al2O3 in the Presence of Water. Langmuir Nov. 2010;26(21):16291–8. https://doi.org/10.1021/la101424a.
[6] Bond JQ, Wang D, Alonso DM, Dumesic JA. Interconversion between γ-valerolactone and pentenoic acid combined with decarboxylation to form butene over silica/alumina. J Catal 2011;281(2):290–9. https://doi.org/10.1016/j.jcat.2011.05.011.
[7] Lange J-P, Price R, Ayoub P, Louis J, Petrus L, Clarke L, et al. Valeric biofuels: a platform of cellulosic transportation fuels. Angew Chemie - Int Ed 2010;49(26):4479–83. https://doi.org/10.1002/anie.201000655.
[8] Contino F, Dagaut P, Dayma G, Halter F, Foucher F, Mounaïm-Rousselle C. Combustion and emissions characteristics of valeric biofuels in a compression ignition engine. J Energy Eng 2014;140(3):1–7. https://doi.org/10.1061/(ASCE)EY.1943-7897.0000161.
[9] Chan-Thaw CE, Marelli M, Psaro R, Ravasio N, Zaccheria F. New generation biofuels: γ-Valerolactone into valeric esters in one pot. RSC Adv 2013;3(5):1302–6. https://doi.org/10.1039/c2ra23043g.
[10] Scotti N, Dangate M, Gervasini A, Evangelisti C, Ravasio N, Zaccheria F. Unraveling the role of low coordination sites in a cu metal nanoparticle: A step toward the selective synthesis of second generation biofuels. ACS Catal 2014;4(8):2818–26. https://doi.org/10.1021/cs500581a.
[11] Martínez Figueredo KG, Segobia DJ, Bertero NM. Influence of the preparation method on the performance of Ni-based bifunctional catalysts in the one-pot conversion of γ-valerolactone to valeric biofuel. Catal Commun 2020;144:106087. https://doi.org/10.1016/j.catcom.2020.106087.
[12] Martínez Figueredo KG, Virgilio EM, Segobia DJ, Bertero NM. Valeric Biofuel Production from γ-Valerolactone over Bifunctional Catalysts with Moderate Noble-Metal Loading. Chempluschem 2021;86(9):1342–6. https://doi.org/10.1002/cplu.v86.910.1002/cplu.202100249.
[13] Bertero NM, Trasarti AF, Apesteguía CR, Marchi AJ. Liquid-phase dehydration of 1-phenylethanol on solid acids: Influence of catalyst acidity and pore structure. Appl Catal A Gen 2013;458:28–38. https://doi.org/10.1016/j.apcata.2013.03.018.
[14] Kozhevnikov IV. Catalysis by heteropoly acids and multicomponent polyoxometalates in liquid-phase reactions. Chem Rev 1998;98(1):171–98. https://doi.org/10.1021/cr960400y.
[15] Bertero NM, Bustos GD, Ferretti CA, Apesteguía CR, Marchi AJ. Liquid phase dehydration of 1-indanol: Selective synthesis of indene over microporous acid catalysts. Micropor Mesopor Mater 2015;213:85–94. https://doi.org/10.1016/j.micromeso.2015.04.019.
[16] Coops J, Jessup RS, van Nes K. No Title. In: Rossini FD, editor. Experimental Thermochemistry. New York: Interscience; 1956. p. 6.
[17] International Zeolite Association. http://www.iza-online.org/.
[18] Díez VK, Marcos BJ, Apesteguía CR, Di Cosimo JI. Ionone synthesis by cyclization of pseudoionone on silica-supported heteropolyacid catalysts. Appl Catal A Gen 2009;358(1):95–102. https://doi.org/10.1016/j.apcata.2009.02.002.
[19] Pizzio LR, Vázquez PG, Cáceres CV, Blanco MN. Supported Keggin type heteropolycompounds for ecofriendly reactions. Appl Catal A Gen 2003;256(1-2):125–39. https://doi.org/10.1016/S0926-860X(03)00394-6.
[20] Wagholikar SG, Niphadkar PS, Mayadevi S, Sivasanker S. Acylation of anisole with long-chain carboxylic acids over wide pore zeolites. Appl Catal A Gen 2007;317(2):250–7. https://doi.org/10.1016/j.apcata.2006.10.023.
[21] Park JN, Wang J, Hong SI, Lee CW. Effect of dealumination of zeolite catalysts on methylation of 2-methylnaphthalene in a high-pressure fixed-bed flow reactor. Appl Catal A Gen 2005;292(1–2):68–75. https://doi.org/10.1016/j.apcata.2005.05.039.
[22] Emeis CA. Determination of integrated molar extinction coefficients for infrared absorption bands of pyridine adsorbed on solid acid catalysts. J Catal 1993;141(2):347–54.
[23] Berhault G, Lacroix M, Breysse M, Maugé F, Lavalley J-C, Nie H, et al. Characterization of acidic sites of silica-supported transition metal sulfides by pyridine and 2,6 dimethylpyridine adsorption: Relation to activity in CH3SH condensation. J Catal 1998;178(2):555–65. https://doi.org/10.1006/jcat.1998.2196.
[24] Ammari F, Lamotte J, Touroude R. An emergent catalytic material: Pt/ZnO catalyst for selective hydrogenation of crotonaldehyde. J Catal 2004;221(1):32–42. https://doi.org/10.1016/S0021-9517(03)00290-2.
[25] Wang J, Huang L, Chen H, Li Q. Acid function of Al-MCM-41 supported platinum catalysts in hydrogenation of benzene, toluene and o-xylene. Catal Lett 1998;55(3–4):157–63. https://doi.org/10.1023/A:1019030811920.
[26] Pappu VKS, Kanyi V, Santhanakrishnan A, Lira CT, Miller DJ. Butyric acid esterification kinetics over Amberlyst solid acid catalysts: the effect of alcohol carbon chain length. Bioresour Technol 2013;130:793–7. https://doi.org/10.1016/j.biortech.2012.12.087.
[27] Tejero MA, Ramírez E, Fité C, Tejero J, Cunill F. Esterification of levulinic acid with butanol over ion exchange resins. Appl Catal A Gen 2016;517:56–66. https://doi.org/10.1016/j.apcata.2016.02.032.
[28] Ferreira P, Fonseca IM, Ramos AM, Vital J, Castanheiro JE. Glycerol acetylation over dodecatungstophosphoric acid immobilized into a silica matrix as catalyst. Appl Catal B Environ 2009;91(1–2):416–22. https://doi.org/10.1016/j.apcatb.2009.06.009.
[29] Yan K, Lafleur T, Wu X, Chai J, Wu G, Xie X. Cascade upgrading of γ-valerolactone to biofuels. Chem Commun 2015;51(32):6984–7. https://doi.org/10.1039/c5cc01463h.
[30] Crépeau G, Montouillout V, Vimont A, Mariey L, Cseri T, Maugé F. Nature, Structure and Strength of the Acidic Sites of Amorphous Silica Alumina: An IR and NMR Study. J Phys Chem B Aug. 2006;110(31):15172–85. https://doi.org/10.1021/jp062252d.
[31] Novodárszki G, Solt HE, Lendvay G, Mihályi RM, Vikár A, Lónyi F, et al. Hydroconversion mechanism of biomass-derived γ-valerolactone. Catal Today 2019;336:50–62. https://doi.org/10.1016/j.cattod.2019.02.020.
[32] Clayborne PA, Nelson TC, DeVore TC. Temperature programmed desorption-FTIR investigation of C 1–C5 primary alcohols adsorbed on γ-alumina. Appl Catal A Gen 2004;257(2):225–33. https://doi.org/10.1016/j.apcata.2003.07.013.
[33] Ward JW, Hansford RC. The detection of acidity on silica-alumina catalysts by infrared spectroscopy-pyridine chemisorption. Relationships between catalyst acidity and activity. J Catal 1969;13(2):154–60. https://doi.org/10.1016/0021-9517(69)90387-X.